This is the accepted manuscript version of the contribution published as:

Pradhan, P., Dutta, R., Zhang, W., Swain, B., Koppa, A., **Kumar, R.**, Karmakar, S., Hari, V. (2025):
North Atlantic forcing on the post-monsoon Arabian Sea cyclones
Earth Syst. Environ. **10** , 4655 - 4670

The publisher's version is available at:

https://doi.org/10.1007/s41748-025-00875-w

North Atlantic Forcing on the Post-monsoon Arabian Sea Cyclones

Pragnya Pradhan[1], Riya Dutta[1], Wei Zhang[2], Basudev Swain[3], Akash Koppa[4], Rohini Kumar[5], Subhankar Karmakar[6,7], Vittal Hari[1*]

[1]Department of Environmental Science and Engineering, Indian Institute of Technology (ISM) Dhanbad, 826004, India.
[2]Department of Plants, Soils and Climate, Utah State University, Utah, USA.
[3]Department of Physics, Atmospheric, Oceanic and Planetary Physics, University of Oxford, UK.
[4]Hydro-Climate Extremes Lab (H-CEL), Faculty of Bioscience Engineering, Ghent University, 9000, Ghent, Belgium.
[5]Department of Computational Hydrosystems, Helmholtz Centre for Environmental Research, Leipzig, Germany.
[6]Interdisciplinary Program in Climate Studies, Indian Institute of Technology Bombay, Mumbai, India.
[7]Environmental Science and Engineering Department, Indian Institute of Technology Bombay, Mumbai, India.

*Corresponding author(s). E-mail(s): vittal@iitism.ac.in; Mobile: +91 9167467068;

Abstract

Recent studies suggests an increased frequency of Arabian Sea (AS) cyclones during post-monsoon season, causing widespread socio-economic damages. Thus, for the improved prediction of these events, understanding the physical mechanism is important which immensely helps in disaster risk management on the western coast of India. Here, using long-term observational data and climate model perturbation experiments, we show that the post-monsoon AS cyclones are influenced by the variability of the North Atlantic Sea Surface Temperature (NASST). NASST significantly reduces vertical wind shear forming a favourable condition for the cyclones to form over the AS. The formation of conditions can be accounted towards alteration in the Walker Circulation. Further, using the Coupled Model Intercomparison Project Phase 6 (CMIP6) models, we show that the conditions in the NASST driving these responses are exacerbated by the greenhouse gas emission, demonstrating that the contribution of anthropogenic influences to NASST variability in recent times outweighs natural variability. If emissions are not contained with proper mitigation measures, a further increase in NASST may also increase the post-monsoon AS cyclonic activities.

1 Introduction

Although only 7% of the total tropical cyclones occurring around the globe originate in the North Indian Ocean (NIO) region (Singh et al., 2001), the massive coastal belt along with the ever-increasing population makes it more vulnerable – in comparison with other Ocean basins – to damages both to life and to the economy of the region (Subrahmanyam et al., 2002). It is reported that most of the cyclones usually form over the Bay of Bengal region, with the Arabian Sea (AS) accounting for 10 – 20% of the total NIO cyclones (Rao et al., 2001). Although the probability of occurrence of cyclones over AS is relatively small compared to the Bay of Bengal (BoB), some of the most severe and damaging cyclones have occurred over the AS in the recent

past (Soltanpour et al., 2021). For example, Cyclone Gonu which occurred from 1–8 June 2007 with maximum wind speeds of 240 km/h (category 5) caused at least 50 deaths and about 4.5 billion USD in damages in Oman and Iran (Fritz et al., 2010). In 2021, the AS experienced Cyclone Tauktae, which was classified as a very severe cyclonic storm, wherein as many as 24 people were killed across three Indian states. More recently, Cyclone Biparjoy, originating in AS during the pre-monsoon season of 2023, was classified as an extremely severe cyclonic storm with a maximum speed of 195km/h, causing damages to the state of Gujarat in India.

The increasing occurrence of cyclones threatens the densely populated coastal regions of the NIO (Malakar et al., 2021). The frequency of occurrence of cyclones falling under the category of extremely severe cyclonic storms has increased over AS in the recent decades (Murakami et al., 2017). For instance, it has been suggested that the cyclone activity over the NIO is increasing due an acceleration of the warming of the NIO (Swapna et al., 2022). This favours an increase in the tropical cyclone intensity (Emanuel, 1986). Specifically, in the AS, mean surface temperature has risen by 1.4°C in recent years compared to the earlier decades (Singh and Roxy, 2022). As a result, the intensification rate of cyclones is much higher in NIO compared to any other oceanic basin (Singh and Roxy, 2022).

Tropical cyclones are driven by complex air-sea interactions, where both atmospheric and oceanic conditions play crucial roles in their formation and intensification. Key environmental factors include sea surface temperature (SST), vertical wind shear, vertical velocity (omega), and relative humidity (RH) (Suneeta and Sadhuram, 2018). However, the relative importance of these factors can vary depending on influences from both local and remote climatic drivers (Hari et al., 2021; Zhang and Villarini, 2019). Previous studies have shown that warming over the Pacific (Girishkumar et al., 2015), Atlantic (Zhang and Villarini, 2019; Hari et al., 2021), and Indian Oceans (Pan and Li, 2008) modulates these cyclone-favouring conditions over the North Indian

Ocean (NIO). For instance, Girishkumar et al. (2015) demonstrated that the combined effects of the El Niño–Southern Oscillation (ENSO) and Madden–Julian Oscillation (MJO) can trigger rapid intensification of tropical cyclones in the Bay of Bengal during the post-monsoon season. Similarly, Krishnamohan et al. (2012) found that the MJO enhances conditions conducive to both genesis and intensification of cyclones across the NIO. Over the AS, the Atlantic Ocean—particularly the southern tropical Atlantic—has been shown to exert a significant influence. Studies by Zhang and Villarini (2019) and Hari et al. (2021) indicate that Atlantic Niño events can modulate the likelihood of pre-monsoon cyclones over the AS. While substantial research has explored the remote influences on Bay of Bengal cyclones and depressions (Mondal et al., 2022; Neetu et al., 2019; Bhalachandran et al., 2019; Anandh et al., 2020), the mechanisms driving cyclone formation over the AS remain relatively understudied.

In the AS, SSTs generally exceed the threshold of 26.5°C required for tropical cyclone development and maintenance (Evan and Camargo, 2011). However, strong vertical wind shear and monsoon-related atmospheric circulation during the summer monsoon season suppress cyclone formation. As a result, cyclones over the AS are largely confined to the pre- and post-monsoon seasons (Rao et al., 2008; Krishna, 2009; Gray, 1968; Evan and Camargo, 2011). Notably, the frequency of cyclone formation is higher in the post-monsoon season compared to the pre-monsoon season (Evan and Camargo, 2011; Evan et al., 2011). Although several studies have explored the physical mechanisms behind pre-monsoon cyclones over the AS (Zhang and Villarini, 2019; Hari et al., 2021), the processes driving post-monsoon cyclone formation remain poorly understood. Attribution studies using climate models have linked the recent rise in post-monsoon AS cyclone frequency to anthropogenic climate change (Evan et al., 2011; Murakami et al., 2017). However, a detailed mechanistic understanding of the large-scale atmospheric conditions that initiate these cyclones is still lacking. This study seeks to address this gap by identifying the key drivers of post-monsoon cyclone

formation over the AS, thereby contributing to improved forecasting and coastal risk management.

Our initial analysis revealed that approx. 54 post-monsoon cyclones occurred over the AS from the period 1981–2022 (Fig. 1a). During the lifetime of these cyclones, we noticed that the north Atlantic Ocean was also anomalously warm (Fig. 1b). A study by Wang et al. (2009) found that the Atlantic Ocean – in general – can induce changes in the Indian Ocean SST variability – specifically along the coast of Africa as well as the western side of the Indian ocean, where the AS exists. Further, a recent study by Zhang and Villarini (2019) also found an influence of Atlantic on the pre-monsoon AS cyclones, suggesting that Atlantic SSTs could be an important factor for post-monsoon AS cyclogenesis. Based on these preliminary analyses, we hypothesize that NASST (70°W–10°E and 0°–44°N) may create conditions favorable for cyclone formation and this study aims to understand the physical mechanisms through which this is favorable for AS cyclone formation through both observational and climate model analyses.

The remainder of the paper is organized as follows. In the present study, the proposed hypothesis was tested by searching evidence of a relationship between the cyclogenesis indices over AS and NASST. For this, we use vertical wind shear and ventilation index as the cyclogenesis indices. Further, to move away from correlation and towards causation, we used climate model perturbation analysis to show that the results from the observations are corroborated well with the perturbation analysis. Finally, we end the article by highlighting the anthropogenic influence on the recent trends in NASST and also analyze the status of NASST in the future, which could potentially explain the frequency of occurrence of AS cyclones in the future.

2 Data and Methods

2.1 Dataset used in the study

To identify the cyclone tracks over the AS, we use the International Best Track Archive for Climate Stewardship (IBTrACS) (Knapp et al., 2010; Gahtan et al., 2024) for the duration of 1981–2022. IBTrACS dataset is based on the best-track data from numerous sources, but for the NIO, the best track information is procured from the India Meteorological Department (IMD; Regional Specialized Meteorological Center's (RSMC), New Delhi) (Levinson et al., 2010). Further, the SST data – both at daily and monthly scale – is procured from the National Oceanic and Atmospheric Administration (NOAA) High-resolution Blended Analysis of Daily SST and Ice which is available at spatial resolution $0.25^\circ \times 0.25^\circ$ (Huang et al., 2021). The NASST is defined over the SST region of 70°W–10°E and 0°–44°N (outlined with a black box in Fig. 1b). To examine large-scale atmospheric circulation patterns (e.g., wind shear, RH, and omega) and to estimate certain cyclone indices, we use data from the NCEP/NCAR Reanalysis-1 project (Kalnay et al., 1996) for the period 1981–2022, available at 2.5° resolution. It should be noted that we have also considered other reanalysis products as well (such as NCEP-NCAR 2 and ERA5) and the results were comparable with the (NCEP-NCAR)-1 and therefore in the main text, we kept (NCEP-NCAR)-1.

Further, to attribute the recent changes in the mechanisms responsible for the AS cyclone (NASST in our case), we procure state-of-the-art global climate model simulations from the CMIP6 (O'Neill et al., 2016). Here we select total 5 CMIP6 models (N=5; ACCESS-CM2, FGOALS-G3, GFDL-ESM4, MIROC6 and MRI-ESM 2.0). The models are selected based on their performance in capturing the observed patterns, i.e., a negative association of vertical wind shear with the NASST over the AS region, along with the fact that these models had the required variable for our analysis in their repository. Further, we selected these models with simulations having a same variant label – primarily r1i1p1f1 – to maintain consistency in ensemble selection. To

quantify the effect of anthropogenic activities in the past (1850 – 2014), four types of forcings are analysed: (1) historical (Hist), (2) natural-only (Hist-NAT), (3) greenhouse gas emission only (Hist-GHG) and (4) aerosol only (Hist-AER). Finally, to assess the condition in the future, we use two Shared Socioeconomic Pathways (SSP) scenarios (SSP 245 and SSP 585), which are available from 2015 – 2100.

2.2 Vertical Wind Shear

Here, we consider wind shear (Corbosiero and Molinari, 2002) as the main factor for TC genesis.

The vertical wind shear (VWS) is calculated with:

$$VWS = \sqrt{(u_{200} - u_{850})^2 + (v_{200} - v_{850})^2} \tag{1}$$

where, u and v are the zonal and meridional wind components, respectively, at 200 and 850 hPa levels. VWS is important for tropical cyclone genesis, because larger VWS may damage the convective structure and subsequently the warm core in the high level of a storm (Korty et al., 2012). It has been reported that a weak VWS tends to facilitate the formation and development of TC (Qi-Zhi and Juan, 2012; Hari et al., 2021; Zhang and Villarini, 2019). In the case, wherein the VWS is stronger, it has been noted that there is an increase of the vertical motion, static instability and RH – caused by the vertical tilting – mainly over the outer region of tropical cyclone. Thus, the convection within the core of a tropical cyclone will be weaker, thereby restricting the development of the warm core and consequently delaying the intensification of cyclone (Qi-Zhi and Juan, 2012). On the other hand, during the condition of weak VWS, an increase in static instability, RH and vertical motion is noticed near the cyclone centre. This condition facilitates an enhancement of vorticity in the cyclone inner-core region and subsequently intensifies the cyclone (Qi-Zhi and Juan, 2012).

2.3 Ventilation Index

Along with wind shear, we also estimate another index, which has been recently introduced by Tang and Emanuel (2012), that is the Ventilation Index (VI). Concerning cyclogenesis, it is believed the formation of the deep moist column, which is hypothesized to be imperative for the spin-up of the vortex, is disrupted by ventilation (Bengtsson et al., 2007; Nolan, 2007; Rappin et al., 2010). The VI serves as a theoretically based metric to assess possible changes in the statistics of tropical cyclones to combined changes in VWS, midlevel entropy deficit, and maximum near-surface wind in climate models (Tang and Emanuel, 2012) – which is defined as the flux of low-entropy air into a tropical disturbance or tropical cyclone (Tang and Camargo, 2014). Further, with respect to genesis, ventilation disrupts the formation of a deep, moist column that is the requirement for the vortex spin up (Emanuel, 1989; Bister and Emanuel, 1997; Rappin et al., 2010). Therefore, the VI has a strong influence on tropical cyclone climatology and the cyclogenesis usually occurs when the VI is anomalously low (Tang and Emanuel, 2012). Based on a theoretical framework, VI includes the parameters VWS, maximum near-surface wind (i.e., V_{max}) and χ and is given by:

$$VI = \frac{VWS \times \chi}{V_{max}} \tag{2}$$

where V_{max} is the maximum near-surface wind, and is approximated by:

$$(V_{max})^2 = \frac{C_K}{C_D} \frac{(T_s - T_o)}{T_o} (h_o^* - h^*) \tag{3}$$

where C_K and C_D are the enthalpy and momentum surface exchange coefficients, respectively. h_o^* is the air saturation enthalpy at the sea surface, whereas h^* is the enthalpy of an ambient boundary layer parcel. Further, $\frac{C_K}{C_D}$ is considered as a constant and set to 0.9 (Wang et al., 2014; Wing et al., 2015). $\frac{(T_s - T_o)}{T_o}$ and $h_o^* - h^*$ represent the tropical cyclone thermodynamic efficiency and thermodynamic disequilibrium, respectively. The VI has a strong influence on tropical cyclone climatology and

the cyclogenesis usually occurs when the VI is anomalously low (Tang and Emanuel, 2012). In addition to these indicators, we also use vertical velocity which plays a crucial role in modulating convection by influencing the rise and fall of air masses promoting the tropical cyclone genesis (Murakami and Wang, 2010).

2.4 Climate model perturbation experiment

We supplement the observational analysis by performing a climate model perturbation experiment, which will further ascertain the role of NASST variability on the AS cyclones and their associated large-scale circulation pattern – through which it influences the AS post-monsoon cyclones. Here, we use the atmospheric general circulation model developed by the International Centre for Theoretical Physics (ICTP AGCM) (Molteni, 2003; Kucharski et al., 2013) – which is found capable of capturing the climatology, including tropical cyclones, over the Indian region (Hari et al., 2021; Dalal et al., 2024; Hari et al., 2024). In the study, we use ICTP AGCM version 41, which has 8 vertical levels, and with a horizontal spectral truncations of T30 (about $3.75^\circ \times 3.75^\circ$ horizontal resolution). Here, we perform the experiment which is integrated over 25 years, with the two sets of independent simulations. In the control experiment, we get a response of atmospheric circulation by prescribing the seasonal climatology of SST (CLIM). Next, this experiment is complemented with the perturbed experiment, wherein we superimpose the warm SST anomalies over the NASST region (the spatially averaged SST over the NASST region is regressed onto the gridded SST field) for October–December on the monthly climatology over the NASST region, keeping the SST identical to the CLIM simulation for other months and other regions. Further, the subtraction of the perturbed simulation with the CLIM simulation provides information about the response of large-scale atmospheric circulation to the NASST – specifically for the post-monsoon season.

2.5 Optimal fingerprinting detection analysis

The methods employed in the study involved conducting an optimal detection analysis utilizing the regularized optimal fingerprinting algorithm (Ribes and Terray, 2013), which was implemented using Python (Kirchmeier-Young et al., 2017). This algorithm, a variant of linear regression, serves to regress the time series of observed NASST changes onto the simulated responses to sets of forcings, such as greenhouse gas (GHG), anthropogenic aerosol (AER), and Natural forcings (NAT), etc.

Mathematically, this can be expressed as;

$$Y = X\beta_i + \varepsilon \tag{4}$$

where, Y represents the observed changes in total NASST, X represents the matrix of simulated responses to sets of forcings, β_i represents the regression coefficients indicating the contribution of each forcing to the observed NASST changes, and ε represents the error term, accounting for internal variability in the climate system. This equation reflects the linear regression framework employed by the algorithm to attribute changes in total NASST to different forcings, such as GHG and NAT, etc.

Moreover, as with Ribes and Terray (2013), we also employ five-year averages aiming to enhance the precision of constraining the natural forcing impact, particularly capturing the rapid response to volcanic eruptions. Further, we estimate the confidence intervals using the regularized optimal fingerprinting algorithm (Ribes and Terray, 2013), to quantify the uncertainty surrounding the estimated response pattern to external forcings. One common method for calculating confidence intervals involves bootstrapping, where resampling techniques are utilized (5000 resamples) to estimate the distribution of the response pattern under different forcings. The confidence interval can be determined based on the percentile range of these resampled response patterns. The 95% confidence interval for each simulations – viz., NAT,

GHG and AER (β_i), is estimated by;

$$\text{CI} = [\beta_i - 1.96 \cdot \text{standard residuals}, \beta_i + 1.96 \cdot \text{standard residuals}]$$

where the standard residuals are estimated from the standard deviation of residuals (Swain et al., 2024). Regarding this confidence interval, the readers can refer to Ribes and Terray (2013) for more details.

2.6 Causal analysis using Bayesian networks

The causal analysis between the cyclone index VI and some important climatic modes such as NASST, AMO and warm Arctic Cold Eurasia pattern (eE) is performed using Graphical Modelling based Bayesian Networks (BNs). BNs are directed acyclic graphs that represent the conditional independence among multiple interacting variables through a set of nodes and edges (Cooper, 1990). The nodes represent the variables and the directed edges represent the association between the variables. The network structure is developed using a score-based hill-climbing greedy search algorithm (Chickering, 2002). In this algorithm, initially, a random network structure is considered as the starting point and a Bayesian Information Criterion (BIC) score (Scanagatta et al., 2018) which represents the fit of a model to the data is estimated. Iteratively, the network structure is randomized by adding, removing, or reversing an edge and the score is re-evaluated in each iteration. The modification that improves the score is retained and the network structure with the maximum BIC score is finally selected. After finalizing the structure, the edge strength which represents the strength of the association between the two variables (nodes), is estimated as the difference between the BIC scores of two network structures, one without and another with the edge. Negative values of the edge strength correspond to a decreased network score

due to the absence of that particular edge. Thus, a more negative difference indicates a stronger relationship between the nodes.

3 Results and Discussion

3.1 Link between NASST and AS large-scale environment

Based on preliminary analysis of observational data (Fig. 1), we found that during the post-monsoon AS cyclones, the SST were anomalously high – specifically over the AS and the North Atlantic. Further, Wang et al. (2009) highlight the North Atlantic as a key driver of SST anomalies globally, exerting a notable influence on the regions such as the NIO. This indicates that NASST may potentially modulate the cyclogenesis over AS during post-monsoon.

Next, we proceed to understand the physical mechanism through which the NASST influences the changes in the atmospheric condition over AS – resulting in cyclones. We begin our analysis with one of the most utilized cyclone indicators, i.e., VWS. Once the cyclone has formed, the VWS decreases the efficiency of the tropical cyclone heat engine by elevating the entrainment of low-entropy parcels into the inner-core convection (Camargo and Zebiak, 2002; Marín et al., 2009) and flushing the boundary layer with downdrafts (Powell, 1990; Riemer et al., 2010). This means a decreased wind shear would favor the cyclone genesis. Here we notice that when the NASST is increased, there is a significant decrease in VWS – specifically over the AS (Fig. 2a) – indicating favourable conditions for the cyclones to occur.

Along with wind shear, we also examine the response of a parameter called entropy deficit – a measure of moisture content in the mid-troposphere – to post-monsoon increase in NASST (see Supplementary information for more details). Fig. S1a shows a significant reduction of the entropy deficit over AS, indicating that the mid-troposphere level is nearing saturation (Emanuel et al., 2008; Huan et al., 2023).

Further, one of the environmental conditions for the weak VWS is the increased vertical velocity (omega), which play an important role in the thermodynamic and dynamic processes of the TC genesis (Shi et al., 2025). When analyzing the response of omega to the increasing NASST, it is noticed that there is a significant decrease in values representing upward motions over AS (Fig. S1b). These conditions along with the decreased VWS subsequently favour the formation of post-monsoon cyclones over AS due to NASST variability.

After having analyzed the response of large-scale atmospheric circulation to NASST, we now proceed to examine how the cyclone - related index responds to the inter-annual variability of NASST. Ventilation – in general – is defined as the flux of low-entropy air into a tropical cyclone (see supplementary information for more details). With respect to increased NASST, we do notice a significant decrease in VI over the AS (Fig. 3a), which indicates that increased NASST are associated with favourable conditions for the formation of cyclone. Even though we found NASST is influencing both the windshear and VI, there could be an influence of intrinsic trend present in the NASST for the results that we have obtained. Therefore, we remove the effect trend and obtain the information pertaining to the inter-annual variability of the NASST and their influence on the cyclonic parameters. Fig. 2b and Fig. 3b shows that even after removing the trend in NASST, we observe a negative association with both the wind shear and VI over the AS, respectively. This further supports our claim that NASST does influence on the formation of cyclones over the AS – specifically during the post-monsoon season. It should be noted that the analysis were performed using NCEP-NCAR 1 reanalysis data, however, when we compared with the other reanalysis products (such as NCEP-NCAR 2 and ERA5), we found a similar results (Fig. S2).

Additionally, along with warmer SST over the northern Atlantic region during AS cyclones, we also observe a warm anomaly over the southern Atlantic Ocean (Fig. 1b)

as well. A recent study by Zhang and Villarini (2019) found that the southern Atlantic Ocean, specifically the Atlantic Nino region (ATL3; Zhang et al. (2023)) does play a significant role in causing the cyclones over the AS – specifically during the pre-monsoon season. Having found the warm anomaly over the ATL3, we perform a similar analysis, as with the NASST. Fig. S3 shows that in general, we notice a significant negative association with both wind shear and VI over AS region similar to NASST. However, when we removed the trend in ATL3, we do not notice any negative association of these two parameters, indicating the relationship with the southern Atlantic Ocean is mostly influenced by the trend, rather than its natural inter-annual variability.

3.2 Mechanistic understanding of NASST teleconnection to AS cyclones

The above analysis shows a significant correlation of NASST with those factors which favour cyclone genesis over the AS – specifically during the post-monsoon season. Next, we investigate the underlying physical mechanism through which NASST could be possibly linked to the AS cyclones. Previous studies suggest that there exists a two-way interaction between the NASST and the NIO (Yang et al., 2022; Chang et al., 2016; Yu et al., 2022). It is reported that the NIO warming increases the warming of SST in North Atlantic by strengthening the outgoing long-wave radiation through atmospheric teleconnection. On the other hand, NASST warming increases the NIO warming due to suppressing the evaporative cooling with weakened surface wind through atmospheric teleconnection (Yang et al., 2022). The atmospheric teleconnection through which these two oceanic basins are connected is explained by Ren et al. (2021), wherein they provide evidence of the weakening of Atlantic Walker circulation. With this backdrop, we analyse the physical mechanisms through which

NASST influences the factors which favour the cyclone over AS – specifically focusing on the Walker circulation, based on the previous studies (Ren et al., 2021). A key variable in this analysis is velocity potential, which serves as a scalar field describing the divergent part of atmospheric circulation and is defined as the inverse Laplacian of divergence, providing a mechanism for broad-scale spatial smoothing (Haltiner and Williams, 1980). At upper levels, such as 200 hPa, negative values of velocity potential represent areas of upper-level divergence and low-level convergence, often indicative of enhanced deep convection (Hendon, 1986). Negative velocity potential anomalies highlight regions of intensified convection, while positive anomalies denote areas of suppressed convection. The climatology of velocity potential at 200 and 850 hPa levels – representing the divergence and convergence at the top of the atmosphere and near-surface level – depicts positive (negative) velocity potential at the Atlantic region at 200 (850) hPa level (Fig. S4). However, on the other hand, we notice negative (positive) values over the east Indian Ocean and also over the Pacific Ocean at 200 (850) hPa level (Fig. S4). The positive (negative) value here in the velocity potential represents the convergence (divergence) behaviour, which is also shown in vectors in Fig. S4. This convergence and divergence pattern over the Atlantic and Indian Ocean – both at the top of the atmosphere and near-surface levels – indicates an Atlantic Walker circulation (Ren et al., 2021). In response to NASST, we notice a substantial change in the climatological patterns of velocity potential. Over the Indian Ocean in general, and the NIO region in specific, we notice an increased divergence (convergence) at the 200 hPa (850 hPa) level (Fig. 4a and b), indicating a weakening of the Walker circulation. The divergence (convergence) at the 200 hPa (850 hPa) level over AS due to the response of NASST also indicates an increase in vertical velocity – which is also evidently shown in Fig. S1b. Based on the results of velocity potential and divergent winds (Fig. S4 and Fig. 4a and b), we propose a schematic diagram of atmospheric teleconnection of NASST on cyclogenesis over AS (Fig. 5). The intense

atmospheric convection (due to the increased convergence at the surface level), and increased moisture input alter the Walker circulation due to the influence of NASST and set the stage congenial for the formation of a cyclone.

Additionally, we explain how these changes in the walker circulation effects the wind shear over the AS. We notice that at the inter-annual timescales (Fig. S5a), the SST over the north Atlantic has shown an increasing trend; on the other hand, the wind shear over the AS during the post-monsoon is decreasing in the recent past and thus the correlation (at 5% significant level) is ≈-0.40 – which is in line with the earlier analysis. Murakami et al. Murakami et al. (2017) further highlight that changes aligned with the climatological mean wind direction, combined with relatively weaker changes in wind speed at certain vertical levels, contribute to the reduction in wind shear. Fig. S5b and c shows the climatological expectations of velocity potential and wind directions during the post-monsoon season over the AS. The climatology of velocity potential at 200 and 850 hPa levels – representing the convergence and divergence at the top of the atmosphere and near-surface level. The wind direction also depicts the westerlies and easterlies in the 200 (850) hPa levels. However, due to the response of NASST, the direction of the winds have changed from westerlies to easterlies in 200 hPa (Fig. S5d) and from easterlies to westerlies at 850 hPa (Fig. S5e). Along with this, we notice a convergence at 850 hPa level (Fig. S5e) and divergence at 200 hPa level (Fig. S5d), due to changes in the Atlantic Walker circulation – as mentioned earlier (please see the schematic diagram). This low-level convergence feeds the cyclone with moist air, while upper-level divergence removes air aloft, maintaining vertical motion and pressure drop. This vertical circulation is the engine of a tropical cycloneJohnson and Yuan (1998); Katz and Zhu (2024). Additionally, when examining the response of wind speed to NASST (Fig. S6a and b), we find a clear difference in magnitude between the 200 hPa and 850 hPa levels. Although wind speeds have generally weakened at both levels, the reduction is substantially greater at 200 hPa compared to 850 hPa

(Fig. S6c). These changes in wind direction, together with the differential weakening of wind speeds between the upper and lower troposphere, lead to a reduction in wind shear over the AS in response to NASST Murakami et al. (2017). We also emphasize that this relationship is most evident at interannual timescales, while the influence of other modes of variability (e.g., decadal variability and forced experiments) remains beyond the scope of this study and may be explored in future research. Overall, it is apparent that the favorable conditions to the response of NASST are formed due to changes in the Atlantic Walker circulation.

3.3 Climate perturbation experiment analysis

In this study, we compare the responses of the large-scale circulation to NASST forcing in climate model perturbation experiment to clarify how inter-annual variability in NASST affects the AS cyclones. By controlling for recent warming trends in the Atlantic, we focus solely on the impacts of NASST variations. Here, we move away from correlation/regression analysis to understanding causation with the implementation of a climate model perturbation experiment. This experiment will take away the effect of the recent warming trend over the Atlantic Ocean (Cheng et al., 2022) thereby isolating the response of only the inter-annual variability of NASST to the AS cyclones. Here, to evaluate the response of the AS cyclones to NASST changes, the regressed quantity of SST over NASST (Fig. 6a) for October–December is superimposed on the seasonal climatology. As with the observational analysis, we also notice that the increased NASST forcing resulted in a substantial reduction in VWS over the AS thus forming a favourable condition for the occurrence of cyclones (Fig. 6b). Further, we assess the underlying physical mechanisms and we notice that due to NASST variability, there is a substantial change in the Walker circulation (Fig. 6c and d), supporting our finding with the observational analysis (Fig. 4a and b). We notice an increased divergence (convergence) at the 200 hPa (850 hPa) level (Fig. 6c and

d) – specifically over the AS. Thus from the climate model perturbation experiment, it is evident that NASST indeed affect the formation of post-monsoon cyclones over AS due to the weakening of the Atlantic Walker circulation. These findings provide a deeper understanding of the ocean-atmosphere interactions that drive cyclone genesis, complementing our observational analysis.

3.4 Attribution analysis and NASST projections

Given the significant role of NASST on the post-monsoon cyclones, we went one step ahead and analysed the role of GHG, NAT and AER on the observed trends in NASST. This will help in explaining the relative role of anthropogenic drivers compared to natural variability in the recent increase in the AS cyclones. Fig. 7a shows the inter-annual variability of post-monsoon NASST for the historical all-forcing, NAT, GHG, and AER only, respectively from the CMIP6 models. We note a striking similarity in variability between historical all-forcings (Hist) and natural-only forcings (Hist-NAT) during the pre-1980 period, indicating the significant role of natural variability on the inter-annual variability of NASST. Post 1980 onwards, however, a similarity between the evolution in the historical all-forcing and GHG experiments is observed. AER forcing, on the other hand, has a inferior (negative), but still not negligible effect on the inter-annual variability of NASST – which is in agreement with previous studies (Li et al., 2022; Sporre et al., 2019). Based on the optimal fingerprinting detection analysis, we found that during pre-1980, NAT forcing led to 0.35–0.57 °C NASST warming contrasting with -0.09–0.17 °C due to GHG forcing. However, during post-1980 – similar to relative importance analysis – we found that GHG forcing has led to 0.56–1.08 °C warming of NASST, forming a primary contributor, followed by NAT forcing with 0.61–0.79 °C.

To further ascertain the role of both NAT and GHG forcings on the NASST, we perform a relative importance analysis (Lindeman et al., 1980; Johnson and LeBreton,

2004) (see Supplementary information for more details), for both pre- and post-1980 (Fig. S7). We found a large contribution of NAT in explaining the variance in historical NASST simulation compared to GHG during pre-1980. However, this scenario changed drastically post-1980, wherein the analysis revealed that the GHG forcing is the major contributor to the inter-annual variability of NASST – in line with the previous studies (Vittal et al., 2020), followed by NAT and AER (being the least important one). Similar observations were obtained when we performed an optimal fingerprinting analysis. During pre-1980, NAT forcing led to 0.35–0.57 °C NASST warming contrasting with -0.09–0.17 °C due to GHG forcing. However, during post-1980 – similar to relative importance analysis – we found that GHG forcing has led to 0.56–1.08 °C warming of NASST, forming a primary contributor, followed by NAT forcing with 0.61 – 0.79 °C. These analyses provide insight into the significant role of anthropogenic activity in causing the recent increase in NASST during the post-monsoon season. The 5 CMIP6 models, could capture the observed pattern satisfactorily (Fig. S8), i.e., both the reduced VWS due to NASST over the AS (Fig. 7b) and also a weakening of the Atlantic Walker circulation (Fig. 7c and d). Further, it is noted that if the GHG emission is not controlled with proper mitigation measures, there will be a further increase in NASST towards the end of the 21st century as shown by SSP 245 and SSP 585 scenarios (Fig. 7e), indicating that there will be a further increase in the frequency of occurrence of the AS cyclones in the future.

3.5 Impact of Supplementary Atlantic Indices on Arabian Sea Cyclogenesis

The SST composite anomaly during the post-monsoon cyclones shows anomalously warm conditions over the Atlantic ocean in general (Fig. 1b). The SST composite anomaly shows a warming pattern similar to that of the AMO, alongside NASST. The AMO is identified as a coherent natural variability mode occurring in the North

Atlantic Ocean at a multi-decadal scale and it controls the variability of the North Atlantic Ocean (Börgel et al., 2020). Along with AMO, we also notice a warming pattern over the equatorial Atlantic SST. Therefore, we have performed a relative importance analysis for both VWS and VI over AS by considering four Atlantic ocean basins, viz., NASST, AMO, equatorial Atlantic SST and Atlantic Nino. Overall, for VWS, we do notice that the NASST does play a leading role in controlling the AS cyclones followed by AMO. Rest of the Atlantic basins had a minimal role in controlling the VWS (Fig. S9a). Similar observation is found when we analyses with the VI (Fig. S9b). From these analysis, it is clear that NASST and AMO play a crucial role and considering these, we perform an additional analysis to see how the AMO is related to the post-monsoon AS cyclones. We notice – as with the NASST – a significant negative association with VI, forming a favorable condition for the cyclone to occur over the AS (Fig. S10a). AMO does not only controls the north Atlantic Ocean but also modulates the conditions over the Arctic region (Fang et al., 2022), and a disjoint study showed that post-monsoon AS cyclones are associated with the warm Arctic conditions (WACE) (Vidya et al., 2023). With this information, we perform an additional analysis by considering WACE and we notice a decreased VI over the AS (Fig. S10b), helping the cyclone genesis over the AS – similar to the study by Vidya et al. (2023). As all these three indices, viz., AMO, NASST and WACE, are connected, it is thus imperative to perform a comprehensive causal analysis (see supplementary information for more details) to identify which parameter plays an important role in causing the AS cyclones. As expected Fig. 8 shows that the AMO and NASST are related to each other, however, we see a direct connection of VI with NASST only. Moreover, it is noticed that NASST is controlling the WACE and the WACE is not significantly associated with the VI over the AS, indicating that the relation between WACE and the post-monsoon AS cyclone – as identified by Vidya et al. (2023) – is rather controlled with NASST, which in turn is controlled by the AMO. Nonetheless,

we believe a comprehensive understanding of this causal network is beyond the scope of the present study and can be considered as potential future research. Moreover, since AMO varies at multi-decadal scale, it would be useful to analyze the century-long changes in the AS cyclones and their association with AMO; and that would be an important extension of this study.

4 Conclusions

The frequency and intensity of post-monsoon cyclones are higher over the AS compared to pre-monsoon (Evan and Camargo, 2011; Evan et al., 2011), and their increased number during the recent periods has been attributed to rising anthropogenic activity (Murakami et al., 2017). Therefore, for proper management of these hazards, one would require information pertaining to both the vulnerability of the region as well as a reliable prediction of the cyclone (Vittal et al., 2020; Dalal et al., 2024). The vulnerability of the region is well documented in the previous studies (Malakar et al., 2021), however, for a reliable prediction of the cyclonic activity it is imperative to understand the causation and their underlying mechanisms (Bellprat et al., 2019). To this end, our study – both by using observational data and climate model perturbation experiments – highlights a link between NASST and large-scale conditions favourable to cyclogenesis over the AS and it does so by weakening the Atlantic Walker circulation.

Thus from these analyses, it is clear that NASST is one of the important factors which can be used for the prediction of cyclones over the AS, and whose value to the cyclone risk management can hardly be overemphasized. Without mitigation measures, continued emissions could drive further increase in NASST, potentially impacting cyclone conditions over AS. However, the specific role of NASST in cyclogenesis remains uncertain due to complex interactions among large-scale atmospheric and oceanic factors. Moreover, the link that is established in the present study is made

theoretical, and however, establishing this link empirically is beyond the scope of the present study and can be considered as a future research work.

Acknowledgements

VH acknowledges support from the DST-SERB (SRG/2022/001376). The authors also acknowledge the efforts of different organizations/people for making the data available for this work which includes NCEP-NCAR reanaysis, International Best Track Archive for Climate Stewardship (IBTrACS) and NOAA High-resolution Blended Analysis of Daily SST and Ice.

Data Availability

Tropical cyclone track and intensity data can be obtained from: IBTrACS (https://www.ncei.noaa.gov/products/international-best-track-archive), temperature and large-scale atmospheric variables – can be downloaded from: NOAA OI SST data (https://www.psl.noaa.gov/data/gridded/data.noaa.oisst.v2.highres.html), NCEP-NCAR reanalysis data (https://psl.noaa.gov/data/gridded/data.ncep.reanalysis.html). The climate indicators used in the present study can be procured from: AMO (https://psl.noaa.gov/data/timeseries/AMO/). CMIP6 model outputs can be acquired from: Earth System Grid Federation nodes (https://esgf-data.dkrz.de/search/cmip6-dkrz/).

Conflict of Interest

The authors have no relevant financial or non-financial interests to disclose.

References

Anandh, T.S., B.K. Das, J. Kuttippurath, and A. Chakraborty. 2020. A coupled model analyses on the interaction between oceanic eddies and tropical cyclones over the bay of bengal. *Ocean Dynamics 70*(3): 327–337 .

Bellprat, O., V. Guemas, F. Doblas-Reyes, and M.G. Donat. 2019. Towards reliable extreme weather and climate event attribution. *Nature Communications 10*(1): 1–7 .

Bengtsson, L., K.I. Hodges, M. Esch, N. Keenlyside, L. Kornblueh, J.J. Luo, and T. Yamagata. 2007. How may tropical cyclones change in a warmer climate? *Tellus A: Dynamic meteorology and oceanography 59*(4): 539–561 .

Bhalachandran, S., R. Nadimpalli, K. Osuri, F. Marks Jr, S. Gopalakrishnan, S. Subramanian, U. Mohanty, and D. Niyogi. 2019. On the processes influencing rapid intensity changes of tropical cyclones over the bay of bengal. *Scientific reports 9*(1): 3382 .

Bister, M. and K.A. Emanuel. 1997. The genesis of hurricane guillermo: Texmex analyses and a modeling study. *Monthly weather review 125*(10): 2662–2682 .

Börgel, F., C. Frauen, T. Neumann, and H.M. Meier. 2020. The atlantic multidecadal oscillation controls the impact of the north atlantic oscillation on north european climate. *Environmental Research Letters 15*(10): 104025 .

Camargo, S.J. and S.E. Zebiak. 2002. Improving the detection and tracking of tropical cyclones in atmospheric general circulation models. *Weather and forecasting 17*(6): 1152–1162 .

Chang, T.C., H.H. Hsu, and C.C. Hong. 2016. Enhanced influences of tropical atlantic sst on wnp–nio atmosphere–ocean coupling since the early 1980s. *Journal of Climate 29*(18): 6509–6525 .

Cheng, L., K. von Schuckmann, J.P. Abraham, K.E. Trenberth, M.E. Mann, L. Zanna, M.H. England, J.D. Zika, J.T. Fasullo, Y. Yu, et al. 2022. Past and future ocean warming. *Nature Reviews Earth & Environment 3*(11): 776–794 .

Chickering, D.M. 2002. Optimal structure identification with greedy search. *Journal of machine learning research 3*(Nov): 507–554 .

Cooper, G.F. 1990. The computational complexity of probabilistic inference using bayesian belief networks. *Artificial intelligence 42*(2-3): 393–405 .

Corbosiero, K.L. and J. Molinari. 2002. The effects of vertical wind shear on the distribution of convection in tropical cyclones. *Monthly Weather Review 130*(8): 2110–2123 .

Dalal, G., T. Pathania, A. Koppa, and V. Hari. 2024. Drivers and mechanisms of heatwaves in south west india. *Climate Dynamics*: 1–15 .

Emanuel, K., R. Sundararajan, and J. Williams. 2008. Hurricanes and global warming: Results from downscaling ipcc ar4 simulations. *Bulletin of the American Meteorological Society 89*(3): 347–368 .

Emanuel, K.A. 1986. An air-sea interaction theory for tropical cyclones. part i: Steady-state maintenance. *Journal of Atmospheric Sciences 43*(6): 585–605 .

Emanuel, K.A. 1989. The finite-amplitude nature of tropical cyclogenesis. *Journal of the Atmospheric Sciences 46*(22): 3431–3456 .

Evan, A.T. and S.J. Camargo. 2011. A climatology of arabian sea cyclonic storms. *Journal of climate 24*(1): 140–158 .

Evan, A.T., J.P. Kossin, C. 'Eddy'Chung, and V. Ramanathan. 2011. Arabian sea tropical cyclones intensified by emissions of black carbon and other aerosols. *Nature 479*(7371): 94–97 .

Fang, M., X. Li, H.W. Chen, and D. Chen. 2022. Arctic amplification modulated by atlantic multidecadal oscillation and greenhouse forcing on multidecadal to century scales. *Nature Communications 13*(1): 1865 .

Fritz, H.M., C.D. Blount, F.B. Albusaidi, and A.H.M. Al-Harthy. 2010. Cyclone gonu storm surge in oman. *Estuarine, Coastal and Shelf Science 86*(1): 102–106 .

Gahtan, J., K.R. Knapp, C.J.I. Schreck, H.J. Diamond, J.P. Kossin, and M.C. Kruk. 2024. International best track archive for climate stewardship (ibtracs) project, version 4.01. *NOAA National Centers for Environmental Information* .

Girishkumar, M., K. Suprit, S. Vishnu, V.T. Prakash, and M. Ravichandran. 2015. The role of enso and mjo on rapid intensification of tropical cyclones in the bay of bengal during october–december. *Theoretical and Applied Climatology* 120: 797–810 .

Gray, W.M. 1968. Global view of the origin of tropical disturbances and storms. *Monthly Weather Review 96*(10): 669–700 .

Haltiner, G.J. and R.T. Williams. 1980. Numerical prediction and dynamic meteorology. *(No Title)* .

Hari, V., A. Pathak, and A. Koppa. 2021. Dual response of arabian sea cyclones and strength of indian monsoon to southern atlantic ocean. *Climate Dynamics 56*(7): 2149–2161 .

Hari, V., O. Rakovec, W. Zhang, A. Koppa, M. Collins, and R. Kumar. 2024. On the role of the atlantic meridional mode in eastern european temperature variability. *Atmospheric Research* 297: 107082 .

Hendon, H.H. 1986. Streamfunction and velocity potential representation of equatorially trapped waves. *Journal of Atmospheric Sciences 43*(23): 3038–3042 .

Huan, D., Q. Yan, and T. Wei. 2023. Unfavorable environmental conditions for tropical cyclone genesis over the western north pacific during the last interglacial based on pmip4 simulations. *Atmospheric and Oceanic Science Letters 16*(5): 100395 .

Huang, B., C. Liu, V. Banzon, E. Freeman, G. Graham, B. Hankins, T. Smith, and H.M. Zhang. 2021. Improvements of the daily optimum interpolation sea surface temperature (doisst) version 2.1. *Journal of Climate 34*(8): 2923–2939 .

Johnson, D. and Z.j. Yuan. 1998. On the forcing of the radial-vertical circulation within cyclones—part 1: Concepts and equations. *Advances in Atmospheric Sciences 15*(3): 346–369 .

Johnson, J.W. and J.M. LeBreton. 2004. History and use of relative importance indices in organizational research. *Organizational research methods 7*(3): 238–257 .

Kalnay, E., M. Kanamitsu, R. Kistler, W. Collins, D. Deaven, L. Gandin, M. Iredell, S. Saha, G. White, J. Woollen, et al. 1996. The ncep/ncar 40-year reanalysis project. *Bulletin of the American meteorological Society 77*(3): 437–472 .

Katz, J. and P. Zhu. 2024. Parameterization of vertical turbulent transport in the inner core of tropical cyclones and its impact on storm intensification. part i: sensitivity to turbulent mixing length. *Journal of the Atmospheric Sciences 81*(10): 1749–1767 .

Kirchmeier-Young, M.C., F.W. Zwiers, and N.P. Gillett. 2017. Attribution of extreme events in arctic sea ice extent. *Journal of Climate 30*(2): 553–571 .

Knapp, K.R., M.C. Kruk, D.H. Levinson, H.J. Diamond, and C.J. Neumann. 2010. The international best track archive for climate stewardship (ibtracs) unifying tropical cyclone data. *Bulletin of the American Meteorological Society 91*(3): 363–376 .

Korty, R.L., S.J. Camargo, and J. Galewsky. 2012. Tropical cyclone genesis factors in simulations of the last glacial maximum. *Journal of Climate 25*(12): 4348–4365 .

Krishna, K.M. 2009. Intensifying tropical cyclones over the north indian ocean during summer monsoon—global warming. *Global and Planetary Change 65*(1-2): 12–16 .

Krishnamohan, K., K. Mohanakumar, and P. Joseph. 2012. The influence of madden–julian oscillation in the genesis of north indian ocean tropical cyclones. *Theoretical and applied climatology* 109: 271–282 .

Kucharski, F., F. Molteni, M.P. King, R. Farneti, I.S. Kang, and L. Feudale. 2013. On the need of intermediate complexity general circulation models: A "speedy" example. *Bulletin of the American Meteorological Society 94*(1): 25–30 .

Levinson, D.H., K.R. Knapp, M.C. Kruk, and J.P. Kossin. 2010. The international best track archive for climate stewardship (ibtracs) project: overview of methods and indian ocean statistics. *Indian ocean tropical cyclones and climate change*: 215–221 .

Li, J., B.E. Carlson, Y.L. Yung, D. Lv, J. Hansen, J.E. Penner, H. Liao, V. Ramaswamy, R.A. Kahn, P. Zhang, et al. 2022. Scattering and absorbing aerosols in the climate system. *Nature Reviews Earth & Environment 3*(6): 363–379 .

Lindeman, R.H., P.F. Merenda, R.Z. Gold, et al. 1980. *Introduction to bivariate and multivariate analysis*, Volume 4. Scott, Foresman Glenview, IL.

669 Malakar, K., T. Mishra, V. Hari, and S. Karmakar. 2021. Risk mapping of indian
670 coastal districts using ipcc-ar5 framework and multi-attribute decision-making
671 approach. *Journal of Environmental Management* 294: 112948 .

672 Marín, J., D. Raymond, and G. Raga. 2009. Intensification of tropical cyclones in the
673 gfs model. *Atmospheric Chemistry and Physics 9*(4): 1407–1417 .

674 Molteni, F. 2003. Atmospheric simulations using a gcm with simplified physical
675 parametrizations. i: Model climatology and variability in multi-decadal experiments.
676 *Climate Dynamics 20*(2): 175–191 .

677 Mondal, M., A. Biswas, S. Haldar, S. Mandal, S. Bhattacharya, and S. Paul. 2022.
678 Spatio-temporal behaviours of tropical cyclones over the bay of bengal basin in last
679 five decades. *Tropical Cyclone Research and Review 11*(1): 1–15 .

680 Murakami, H., G.A. Vecchi, and S. Underwood. 2017. Increasing frequency
681 of extremely severe cyclonic storms over the arabian sea. *Nature Climate*
682 *Change 7*(12): 885–889 .

683 Murakami, H. and B. Wang. 2010. Future change of north atlantic tropical
684 cyclone tracks: Projection by a 20-km-mesh global atmospheric model. *Journal of*
685 *Climate 23*(10): 2699–2721 .

686 Neetu, S., M. Lengaigne, J. Vialard, G. Samson, S. Masson, K. Krishnamohan, and
687 I. Suresh. 2019. Premonsoon/postmonsoon bay of bengal tropical cyclones intensity:
688 Role of air-sea coupling and large-scale background state. *Geophysical research*
689 *letters 46*(4): 2149–2157 .

690 Nolan, D.S. 2007. What is the trigger for tropical cyclogenesis. *Australian*
691 *Meteorological Magazine 56*(4): 241–266 .

O'Neill, B.C., C. Tebaldi, D.P. Van Vuuren, V. Eyring, P. Friedlingstein, G. Hurtt, R. Knutti, E. Kriegler, J.F. Lamarque, J. Lowe, et al. 2016. The scenario model intercomparison project (scenariomip) for cmip6. *Geoscientific Model Development 9*(9): 3461–3482 .

Pan, L.L. and T. Li. 2008. Interactions between the tropical iso and midlatitude low-frequency flow. *Climate dynamics* 31: 375–388 .

Powell, M.D. 1990. Boundary layer structure and dynamics in outer hurricane rainbands. part ii: Downdraft modification and mixed layer recovery. *Monthly Weather Review 118*(4): 918–938 .

Qi-Zhi, C. and F. Juan. 2012. Effects of vertical wind shear on intensity and structure of tropical cyclone. *Journal of Tropical Meteorology 18*(2) .

Rao, D.B., C. Naidu, and B.S. Rao. 2001. Trends and fluctuations of the cyclonic systems over north indian ocean. *Mausam 52*(1): 37–46 .

Rao, V.B., C.C. Ferreira, S. Franchito, and S. Ramakrishna. 2008. In a changing climate weakening tropical easterly jet induces more violent tropical storms over the north indian ocean. *Geophysical research letters 35*(15) .

Rappin, E.D., D.S. Nolan, and K.A. Emanuel. 2010. Thermodynamic control of tropical cyclogenesis in environments of radiative-convective equilibrium with shear. *Quarterly Journal of the Royal Meteorological Society 136*(653): 1954–1971 .

Ren, S.M., S.Q. Zhang, L. Lu, Y.J. Jiang, and Y.W. Ma. 2021. Impact of tropical atlantic warming on the pacific walker circulation with numerical experiments of cgcm. *Advances in Climate Change Research 12*(6): 757–771 .

Ribes, A. and L. Terray. 2013. Application of regularised optimal fingerprinting to attribution. part ii: application to global near-surface temperature. *Climate dynamics* 41: 2837–2853 .

Riemer, M., M.T. Montgomery, and M.E. Nicholls. 2010. A new paradigm for intensity modification of tropical cyclones: Thermodynamic impact of vertical wind shear on the inflow layer. *Atmospheric Chemistry and Physics 10*(7): 3163–3188 .

Scanagatta, M., G. Corani, C.P. De Campos, and M. Zaffalon. 2018. Approximate structure learning for large bayesian networks. *Machine Learning* 107: 1209–1227 .

Shi, Y., L. Zhang, and Y. Du. 2025. Enso modulating tropical cyclone geneses in fall and winter seasons over the south china sea. *Theoretical and Applied Climatology 156*(1): 1–13 .

Singh, O., T.M.A. Khan, and M.S. Rahman. 2001. Has the frequency of intense tropical cyclones increased in the north indian ocean? *Current science*: 575–580 .

Singh, V.K. and M. Roxy. 2022. A review of ocean-atmosphere interactions during tropical cyclones in the north indian ocean. *Earth-Science Reviews* 226: 103967 .

Soltanpour, M., Z. Ranji, T. Shibayama, and S. Ghader. 2021. Tropical cyclones in the arabian sea: overview and simulation of winds and storm-induced waves. *Natural Hazards* 108: 711–732 .

Sporre, M.K., S.M. Blichner, I.H. Karset, R. Makkonen, and T.K. Berntsen. 2019. Bvoc–aerosol–climate feedbacks investigated using noresm. *Atmospheric Chemistry and Physics 19*(7): 4763–4782 .

Subrahmanyam, B., K. Rao, N. Srinivasa Rao, V. Murty, and R.J. Sharp. 2002. Influence of a tropical cyclone on chlorophyll-a concentration in the arabian sea.

Geophysical Research Letters 29(22): 22–1 .

Suneeta, P. and Y. Sadhuram. 2018. Tropical cyclone genesis potential index for bay of bengal during peak post-monsoon (october-november) season including atmosphere-ocean parameters. *Marine Geodesy 41*(1): 86–97 .

Swain, B., M. Vountas, A. Singh, and S.S. Gunthe. 2024. Tracing human influence on rising surface air temperature in venezuela. *Scientific Reports 14*(1): 28005 .

Swapna, P., P. Sreeraj, N. Sandeep, J. Jyoti, R. Krishnan, A. Prajeesh, D. Ayantika, and S. Manmeet. 2022. Increasing frequency of extremely severe cyclonic storms in the north indian ocean by anthropogenic warming and southwest monsoon weakening. *Geophysical Research Letters 49*(3): e2021GL094650 .

Tang, B. and S.J. Camargo. 2014. Environmental control of tropical cyclones in cmip5: A ventilation perspective. *Journal of Advances in Modeling Earth Systems 6*(1): 115–128 .

Tang, B. and K. Emanuel. 2012. A ventilation index for tropical cyclones. *Bulletin of the American Meteorological Society 93*(12): 1901–1912 .

Vidya, P., S. Chatterjee, M. Ravichandran, S. Gautham, M. Nuncio, and R. Murtugudde. 2023. Intensification of arabian sea cyclone genesis potential and its association with warm arctic cold eurasia pattern. *npj Climate and Atmospheric Science 6*(1): 146 .

Vittal, H., S. Karmakar, S. Ghosh, and R. Murtugudde. 2020. A comprehensive india-wide social vulnerability analysis: highlighting its influence on hydro-climatic risk. *Environmental Research Letters 15*(1): 014005 .

Vittal, H., G. Villarini, and W. Zhang. 2020. On the role of the atlantic ocean in exacerbating indian heat waves. *Climate dynamics 54*(3): 1887–1896 .

Wang, C., F. Kucharski, R. Barimalala, and A. Bracco. 2009. Teleconnections of the tropical atlantic to the tropical indian and pacific oceans: A review of recent findings. *Meteorologische Zeitschrift 18*(4): 445–454 .

Wang, S., S.J. Camargo, A.H. Sobel, and L.M. Polvani. 2014. Impact of the tropopause temperature on the intensity of tropical cyclones: An idealized study using a mesoscale model. *Journal of the Atmospheric Sciences 71*(11): 4333–4348 .

Wing, A.A., K. Emanuel, and S. Solomon. 2015. On the factors affecting trends and variability in tropical cyclone potential intensity. *Geophysical Research Letters 42*(20): 8669–8677 .

Yang, Y.M., J.H. Park, S.I. An, S.W. Yeh, Z. Zhu, F. Liu, J. Li, J.Y. Lee, and B. Wang. 2022. Increased indian ocean-north atlantic ocean warming chain under greenhouse warming. *Nature communications 13*(1): 3978 .

Yu, T., J. Feng, W. Chen, and S. Chen. 2022. The interdecadal change of the relationship between north indian ocean sst and tropical north atlantic sst. *Journal of Geophysical Research: Atmospheres 127*(16): e2022JD037078 .

Zhang, L., C. Wang, W. Han, M.J. McPhaden, A. Hu, and W. Xing. 2023. Emergence of the central atlantic niño. *Science Advances 9*(43): eadi5507 .

Zhang, W. and G. Villarini. 2019. On the role of the atlantic ocean in forcing tropic cyclones in the arabian sea. *Atmospheric research* 220: 120–124 .

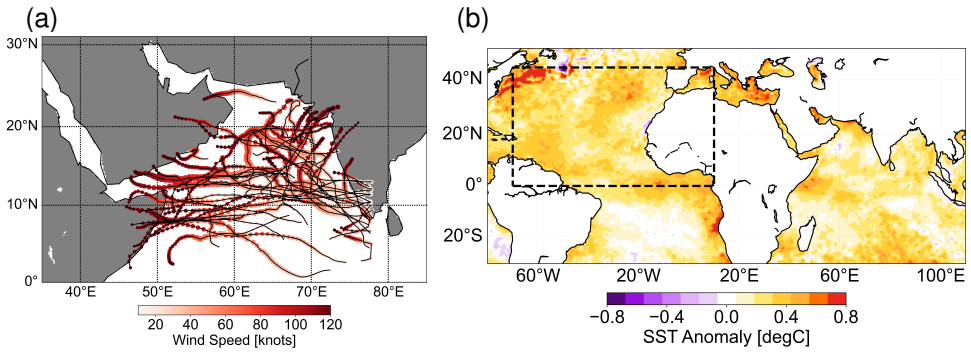


Fig. 1 Cyclones over the AS during post-monsoon season (October–December) and the associated SST anomaly. (a) Tracks of the tropical cyclones (N=54) during 1981–2022. (b) Oceanic conditions during the post-monsoon AS cyclones – wherein we show composite SST anomalies during the AS cyclones. Here, composite anomaly is constructed by considering the SST condition during the cyclone lifetime that are subtracted with their respective climatological condition (1981–2022). Dashed black box indicates the NASST region (70°W–10°E and 0°–44°N; and spatially averaging SST over this region is our NASST index).

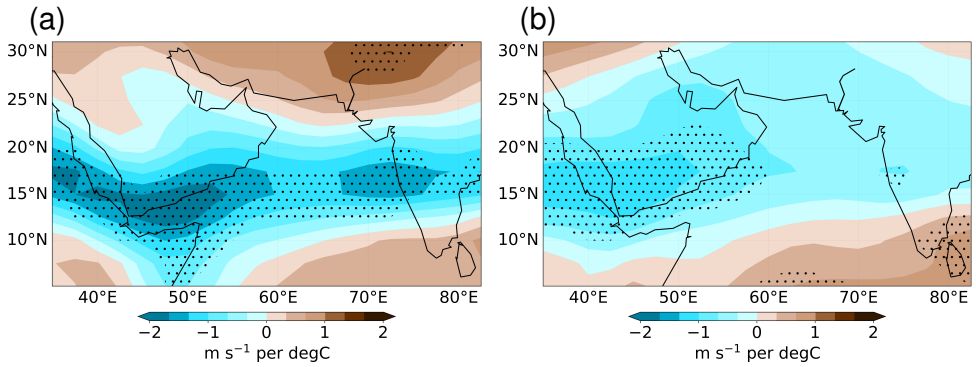


Fig. 2 Large-scale atmospheric circulation pattern (a) Regression of wind shear to NASST index during 1981–2022 in the NCEP reanalysis. The dotted region in these figures represent the region wherein the slopes are statistically significant at 5% significance level. (b) is same as (a), but with the de-trended NASST. The dotted region in this figures represent the region wherein the slopes are significant at 10% significance level.

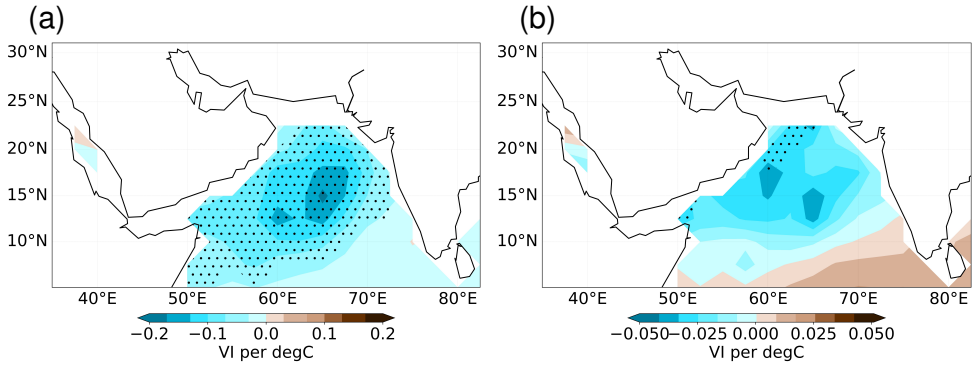


Fig. 3 Same as Figure 2, but for the ventilation index

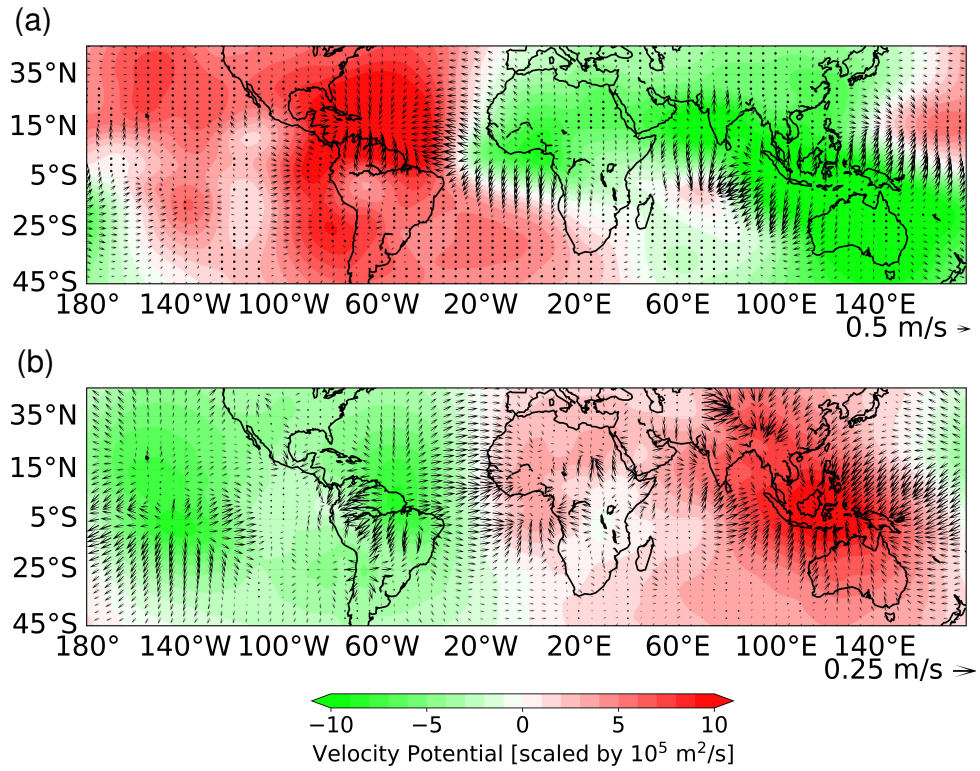


Fig. 4 Physical mechanisms associated with NASST Regression of post-monsoon velocity potential (shaded) and the divergent winds (vectors) to NASST during 1981–2022 (a) at 200 hPa level. (b) is the same as (a), but for the 850 hPa level. The negative (positive) values indicate the region with divergence (convergence). The vectors in the figure represent the winds.

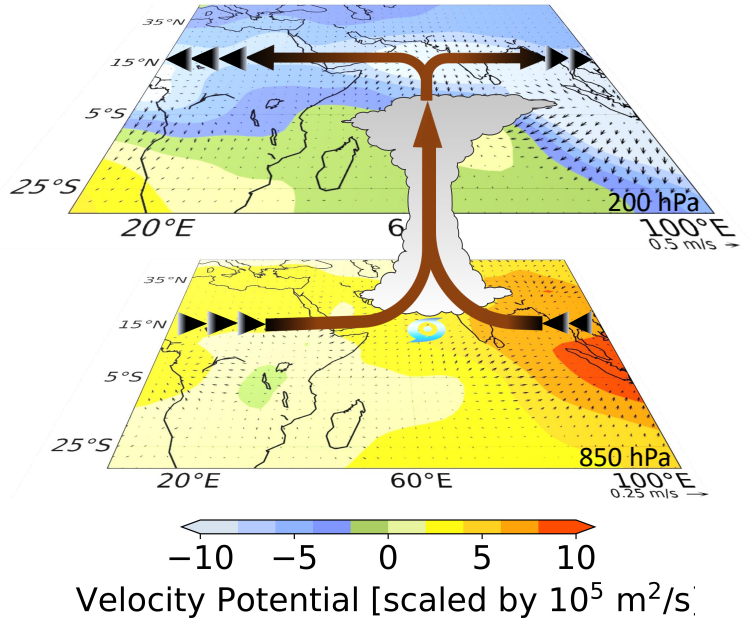


Fig. 5 Schematic diagram of NASST remotely impacting on the AS cyclogenesis.

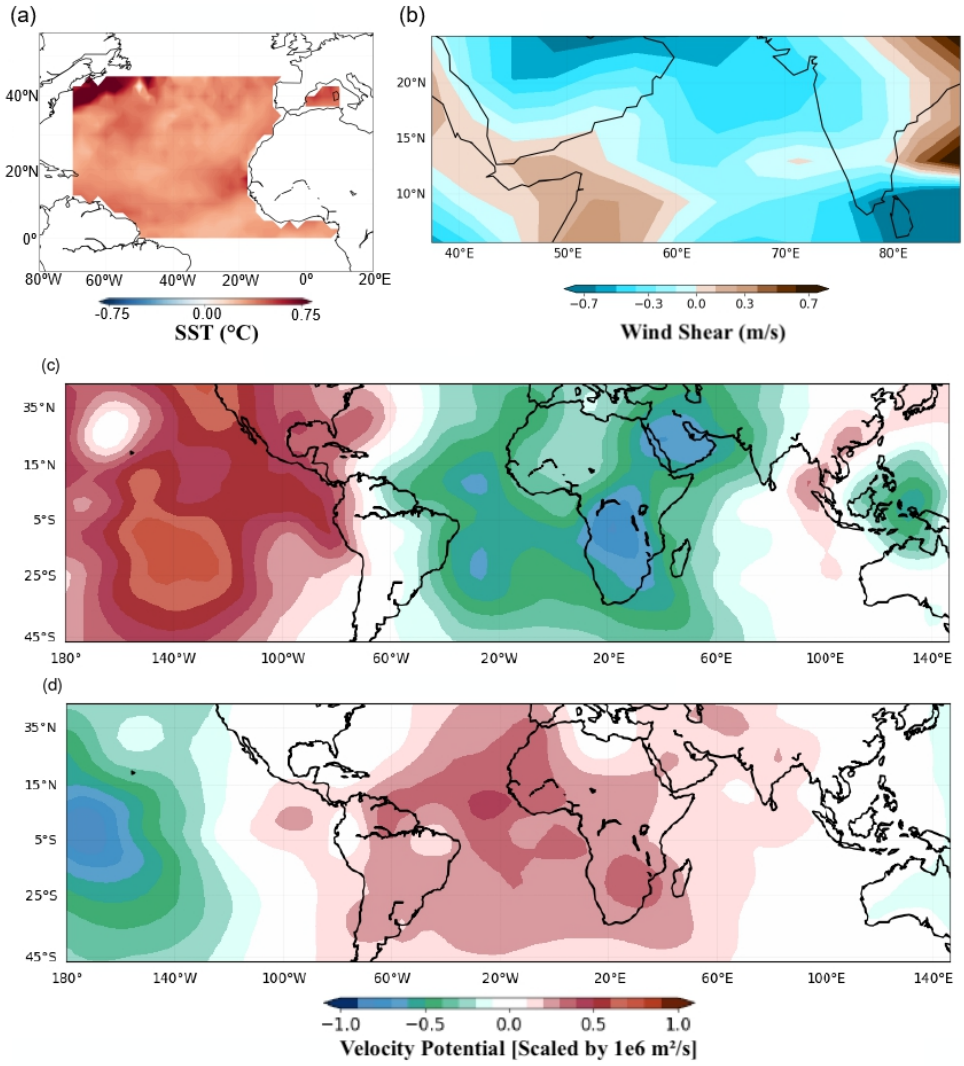


Fig. 6 Climate model perturbation experiment. (a) Anomalies that were added to the climatological SSTs in the perturbation experiment. (b) Response of wind shear to the perturbation experiment forced with NASST anomalies. Responses of velocity potential both at 200 (c) and 850 hPa (d) levels to the perturbation experiment forced with NASST anomalies, wherein the negative (positive) values indicate the region with divergence (convergence).

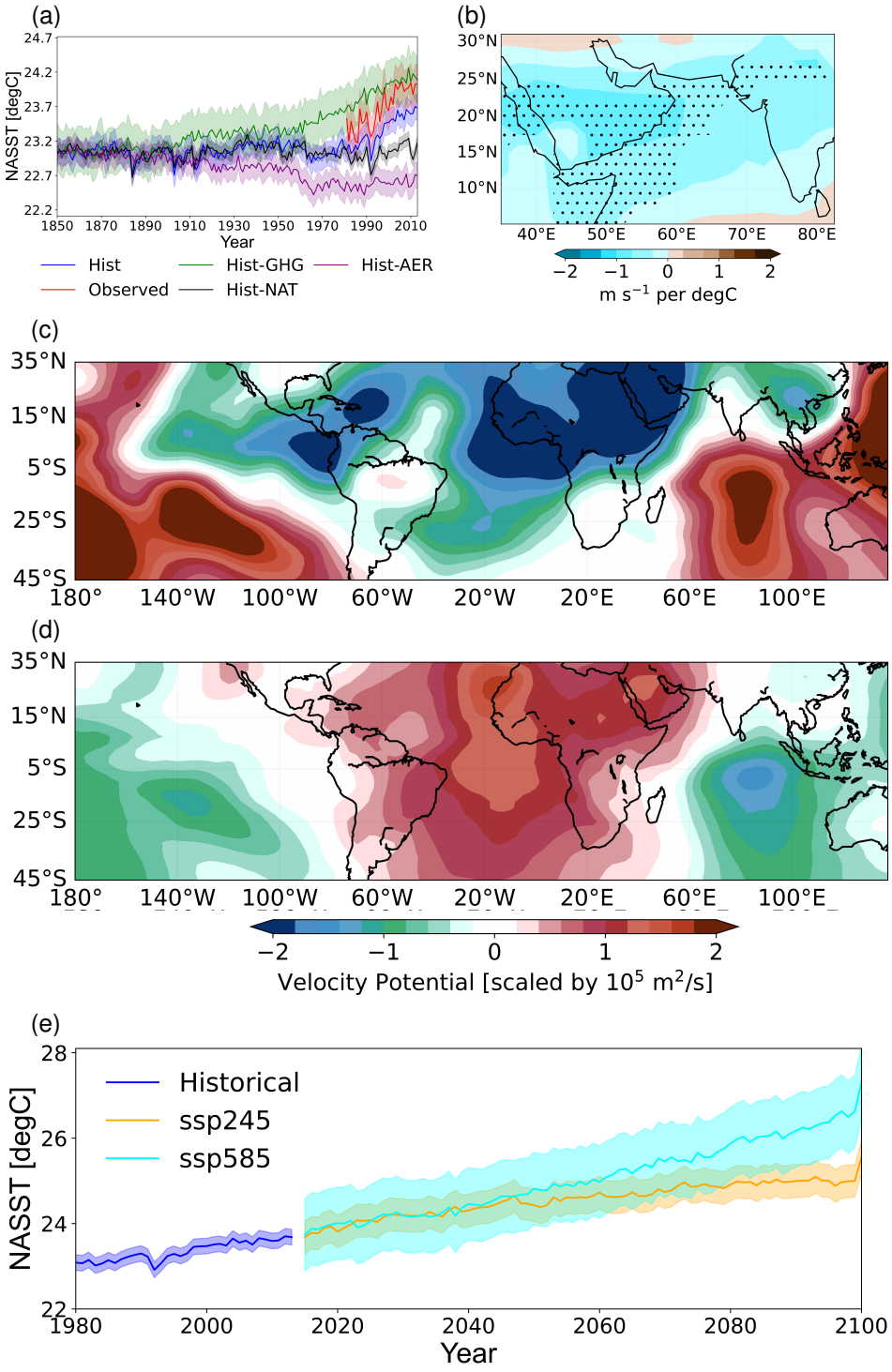


Fig. 7 (a) Inter-annual variability of NASST based on the CMIP6 all-forcing historical experiment (blue), NAT only (black), GHG only (green), AER only (purple) and from the observational data (red). The thick line shows the multi-model mean (N=5) and the filled areas around the thick line represent the one standard deviation based on the six selected models in this study. (b) Regression of wind shear to the NASST – provided in terms of multi-model mean – for the post-monsoon season during the period 1981 – 2014. (c) and (d) are the same as (b), but for the velocity potential at 200 and 850 hPa levels, respectively. (e) Yearly variation of the NASST for the historical (from 1981 – 2014) and for the two future scenarios, i.e., for SSP 245 (brown) and SSP 585(cyan), respectively.

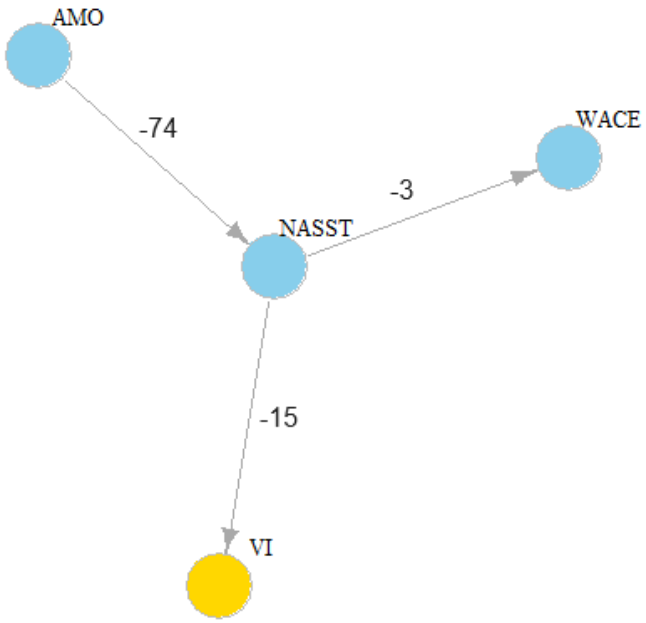


Fig. 8 Network or conditional independence structure showing the association between the ventilation index and the three causal variables (NASST, WACE and AMO). The strength of association between variables is also indicated along the significant edges (a 'more negative' value represents a 'stronger association'.